



Research Article

Experimental investigation of heat transfer characteristics of an inverse diffusion flame in a coaxial tube burner for with and without swirl

Shankar BADIGER^{1,*}, V.V. KATTI¹, T.R. ANIL²

¹Department of Mechanical Engineering, KLS, VDIT, Haliyal, India

²Department of Aeronautical Engineering, KLS, GIT, Belagavi, India

ARTICLE INFO

Article history

Received: 30 March 2020

Accepted: 22 July 2020

Keywords:

Coaxial Tube Burner; Radial Heat Flux; Inverse Diffusion Flame; Twisted Tape; Thermal Imager

ABSTRACT

Heat transfer by flame jet impingement is widely used in many of the industrial and domestic applications like heating metal bars, scrap melting, shaping the glass, metal slab cutting, domestic cooking and others. Aim of the present experimental work is to study an effect of swirl on a local heat flux distribution of an inverse diffusion flame (IDF) jet impinging on a flat target surface in a coaxial tube burner. The twisted tape of twist ratio 3 (corresponding to the swirl number, $S = 0.52$) is used to create a swirl in the central air jet of the burner. The flame shapes and heat flux distributions are compared for the with and without swirling IDF under the different air jet Reynolds number (Re_a) of 1000 to 2500, equivalence ratio (ϕ) of 0.4 to 1.3 and a burner-to-impingement plate distance (H) of 10 to 100mm. The distributions of heat fluxes are studied within a radius of 75 mm from the point of stagnation on an impingement plate. Results show that the swirling IDF helps in clean combustion of the fuel with much shorter flame height. Swirling in the flame jet enhances the peak heat flux for the higher air jet Reynolds number for slightly fuel rich conditions of $\phi = 1.1$ at the optimal burner-to-target plate distance of 40 mm.

Cite this article as: Shankar B, Katti V V, ANIL T R. Experimental investigation of heat transfer characteristics of an inverse diffusion flame in a coaxial tube burner for with and without swirl. J Ther Eng 2022;8(1):67–77.

INTRODUCTION

Gaseous combustion is used in industries for many of the applications due their better convective heat transfer. By considering the safety and wide range of flame stability limits in comparison to premixed combustion, the diffusion flames are used in industries. The inverse diffusion flame is obtained in a co-axial tube burner having a central

air jet with annular space of fuel jet surrounding the air jet. The entrainment of fuel into the air jet results in better mixing and burning. Sze et al. [1] studied flame shapes, thermal and emission characteristics of two different IDF burners. Mikofski et al. [2] investigated the flame heights for varying air flow rates. The experimentation on the

*Corresponding author.

*E-mail address: badiger1185@gmail.com, katti.vadiraj@gmail.com, tranil@git.edu

This paper was recommended for publication in revised form by Regional Editor Hasan Köten



liquid petroleum gas (LPG) flame structure in a backstep IDF tube burner is carried out by Mahesh and Mishra [3,4]. They observed blue flame when air jet speed is increased. Zhen et al. [5] varied the nozzle length of IDF burner and found good performance with shorter nozzle. Dong et al. [6] examined the effect of an air jet diameter of an IDF burners and investigated the thermal and emission characteristics. Choy et al. [7] examined the pollutant emissions of an IDF. The emissions of LPG combustion in an IDF burner is carried out with the addition of hydrogen by Miao et al. [8]. Cha et al. [9] focused on a recirculating flow structure of a normal diffusion flame and compared with numerical simulation.

Due to better combustion characteristics, the swirling flames are becoming important in practical applications. Zhen et al. [10] studied the flame shapes of an IDF burner by creating swirl in the flame. It is observed that the internal recirculation zone in the flame which stabilizes and shortens the flame. Kotb and Saad [11] experimented with the swirl burners to examine the thermal and pollutants of an IDF. An effect of swirl vane angle and a number of swirl vanes on thermal and emission characteristics of an IDF have been investigated by Patel and Shah [12,13]. Basem A. Rabee [14] studied the effect of an air jet diameter on the thermal and emission characteristics of an IDF. Patel and Shah [15] examined the effect of swirler vane angle on the flame appearance and CO emissions of the LPG diffusion flame. The results exhibited that the higher flame stability with less CO is attained with the help of swirl. Tong et al. [16] conducted an experiment to study the structure of flames and emissions of a diffusion flames stabilized by swirling flow and bluff-body. An experimental result is then compared with numerical simulations.

The premixed flames and inverse diffusion flames are used in heating applications due to its better convective heat transfer. Many of the researchers examined the heat transfer rate of swirling premixed flames. [17-21]. They observed higher heat flux with better uniformity on the target surface by the swirling flame jet. Sze et al. [22] carried out the parametric study on an IDF burner to investigate the heat flux. They reported that more uniform heating is observed at a stagnation point as compared to premixed impingement. Dong et al. [23,24] conducted experiments with different air jet diameter IDF burners and studied heat flux on the target surface. H.S. Zhen et al. [25,26] are only the researchers who introduced swirl in an IDFs and investigated the heat flux on the target plate. The swirl in an IDF burner was established by two tangential air inlets connected to a swirl chamber, tangential air entry induced the rotational motion in an air jet. In the literature it is observed that the swirling in the flame jet improves the thermal and emissions characteristics of an IDF and also enhanced the impingement heat transfer. This motivates the author to focus on the swirling inverse diffusion flame jet as there is a limited study is available on the swirling IDF impingement heat transfer.

It is also seen that there is no information available in the literature using twisted tape as a swirler to investigate the swirling flame jet heat transfer behaviour of an IDF. In the present work, the local heat transfer distributions in a radial location on an impingement plate is studied by the novel method of inverse heat conduction problem (IHCP) in a semi-infinite medium using a thermal imager. The radial heat flux distribution is presented for an air jet Reynolds number (Re_a) of 1000 to 2500, an equivalence ratio (ϕ) of 0.4 to 1.3 and burner-to-impingement plate distance (H) of 10 to 100 mm. The objectives of the present experimental work are outlined:

- 1) To study the flame shapes.
- 2) To study the radial heat flux distribution of swirling inverse diffusion flame in a coaxial tube burner.
- 3) To compare the radial heat flux values on an impingement surface for the with and without swirling inverse diffusion flame jet.

EXPERIMENTAL METHOD

Figure 1(a) illustrates the schematic diagram of the coaxial tube burner used in this work. The burner consists of two concentric tubes with an inner tube of 5mm in diameter and an outer tube of 10mm in diameter. The burner is operated with the central air jet and being surrounded with the annular fuel jet. The fuel comes out with an annular slit of 1.9mm. The burner is provided with a sufficient L/d_a ratio of greater than 20 to achieve the fully developed flow. In order to study an effect of swirl on the flame appearance and local heat transfer characteristics, the twisted tape of 15mm pitch with a twist ratio of 3 is used in an experimental work and is shown in fig. 1(b). The twisted tape fit inside an air jet tube. The swirl number (S), which characterizes the degree of swirl and is obtained by an equation (2). The value of swirl number (S) is 0.52 for the twisted tape of 15mm pitch.

Figure 2 illustrates the schematic representation of an experimental setup. The constant pressure air is supplied to the coaxial tube burner from an air screw compressor. The mass flow rate of a constant pressure air is controlled by a needle valve. The flow rate of an air is measured by a calibrated orifice meter incorporated in an air line. The experiments are conducted using the methane fuel of 99.99% purity. The flow rate of fuel is controlled by a needle- valve and metered by a calibrated orifice meter. An enclosure is provided to the burner to avoid the disturbances from the surrounding. A glass window is provided at the front to visualize the IDF. A flat plate is used as a target plate in the **present** study. The target surface is made up of quartz plate of size 150mm x 150mm and 3mm thickness with an emissivity of 0.93[18]. The temperature distribution on the quartz plate is obtained with the help of a thermal imager (Fluke Ti400) and the specifications are given in the table 1. The heat flux on the target surface

is calculated by an equation (5) by an inverse heat conduction method problem [18, 27].

An uncertainty in the heat flux is found 10% as calculated by Moffat RJ [28] and is estimated as

$$q'' = \frac{T(z,t) - T_i}{\frac{2\sqrt{\alpha t/\pi}}{k} \exp\left(\frac{-Z^2}{4\alpha t}\right) - \frac{Z}{k} \operatorname{erfc}\left(\frac{Z}{2\sqrt{\alpha t}}\right)} \quad (1)$$

Assuming that an uncertainty in material thermal properties (α and k) are negligible, an uncertainty in the heat flux is given by

Table 1. Thermal imager specifications used in the experimental work

Model	Fluke Ti-400
Detector type	Focal plane array, Uncooled
Spectral range	7.5–14 μm
Pixel resolution	320 \times 240 pixels
Minimum focus distance	15 cm
Temperature range	–20°C to 1200°C
Accuracy	$\pm 2^\circ\text{C}$

$$\frac{dq''}{q''} = \sqrt{\left(\frac{\Delta T}{T(z,t) - T_i}\right)^2} \quad (2)$$

The swirl number, S is defined as

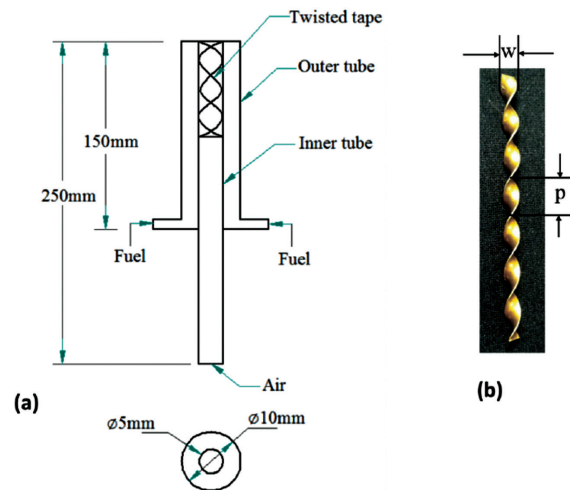
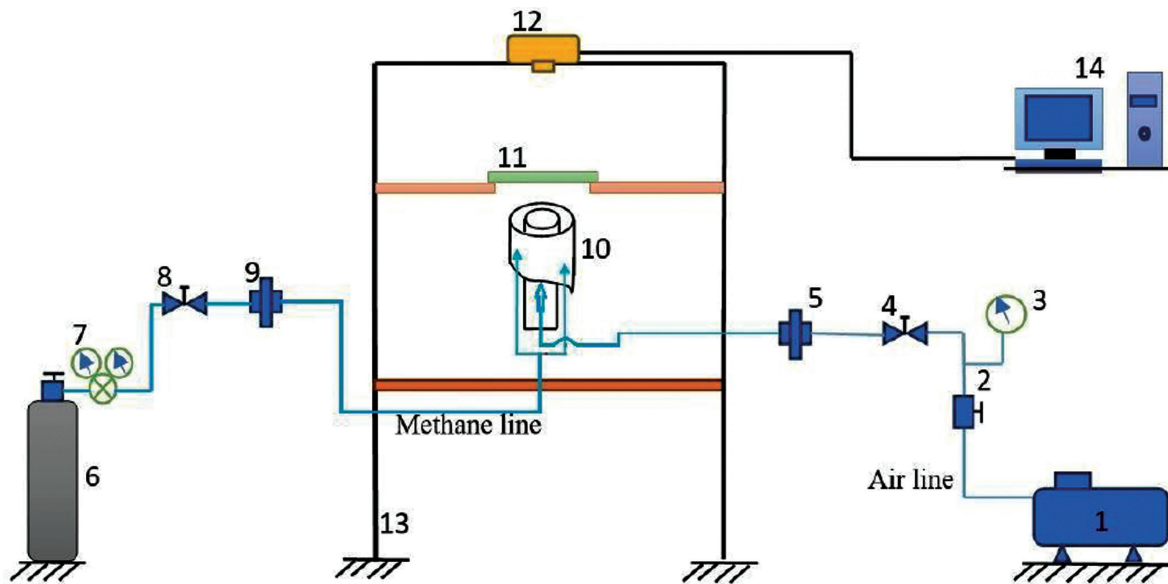


Figure 1. (a) Coaxial burner geometry. (b) Twisted tape.



- | | | |
|-----------------------|------------------------|--------------------------|
| 1. Air compressor | 6. Methane cylinder | 11. Quartz plate |
| 2. Pressure regulator | 7. Two-stage regulator | 12. Thermal camera |
| 3. Pressure Gauge | 8. Needle valve | 13. Supporting structure |
| 4. Needle valve | 9. Methane flowmeter | 14. Personal computer |
| 5. Air Flowmeter | 10. Coaxial burner | |

Figure 2. Schematic diagram of the experimental setup.

$$S = \pi / (2(TR)) \quad (3)$$

Where, $TR = p/w$

The equivalence ratio, ϕ is defined as

$$\phi = (\dot{m}_a / \dot{m}_f)_{stoic} / (\dot{m}_a / \dot{m}_f)_{act} \quad (4)$$

The Reynolds number (Re_a) corresponding the air jet velocity in the air-port tube of an IDF burner is calculated as

$$Re_a = (4\dot{m}_a) / (\pi d_a \mu_a) \quad (5)$$

The heat flux is acquired on the target plate by treating it as a semi-infinite model. For the constant heat flux, the temperature distribution $T(z,t)$ on the backside of the target plate with the time (t) at a depth of Z in semi-infinite medium is obtained by the following equation:

$$T(z,t) - T_i = \frac{2q''\sqrt{\alpha t/\pi}}{k} \exp\left(\frac{-Z^2}{4\alpha t}\right) - \frac{q''Z}{k} \operatorname{erfc}\left(\frac{Z}{2\sqrt{\alpha t}}\right) \quad (6)$$

The infrared thermal camera is used to record the distribution of temperature on the back surface of the quartz plate. For the short interval of time and by fluctuating the heat flux (q''), for different time intervals, the noted temperature $T(z,t)$ is then matched with an equation (6), such that the square root of the sum of squares, $RSS = \sqrt{\sum_{i=1}^n (T_{analytical} - T_{experimental})^2}$ is minimum [18,27]. The uncertainties are calculated by the procedure given by the Moffat [25] and are found to be 10% for estimated heat flux.

RESULTS AND DISCUSSION

The distribution of heat flux along the radius on the target surface is studied for a different air jet Reynolds number

(Re_a) from 1000 to 2500, an equivalence ratio (ϕ) from 0.4 to 1.3 and the normalized distance between burner- to-target plate (H) from 10 to 100mm. A comparison is made for the inverse diffusion flames of the coaxial tube burner with and without swirl conditions by the twisted tape inserted in the air jet. The impinging flame shapes are studied.

Impinging Flame Shapes

The photos of an impinging flames of an inverse diffusion flame coaxial tube burner at varying Re_a , varying ϕ , and varying H are shown in the figs. 3 to 5 respectively for the swirl and non-swirling conditions. Fig. 3 shows an impinging flame shapes for the swirl and without swirl conditions at $\phi = 1.1$, $H = 20$ mm and for $Re_a = 1000$ to 2500. The flame exhibits blue colour at the base and at the boundary layer of the flame due to the combustion with the help of surrounding air. The soot is observed at the contracted region of the flame, indicated by yellow/orange colour which represents the mixing region. The intensity of soot is higher at lower Re_a and subsequently decreases when Re_a is increased to 2500. Both air and fuel flow rates increase when Re_a is increased at a fixed ϕ . Higher the Re_a results in the stronger mixing of air and fuel which promotes the complete combustion of fuel. An introduction of swirl with the help of twisted tape creates the turbulence which leads to the intense mixing of air and fuel and results in better combustion. At the higher Re_a of 2500, IDF exhibits a dual structure flame with a shorter base flame, neck region and post combustion zone impinging the plate. The similar flame structure is reported by Zhen et al. [26].

Figure 4 shows an impinging flame shapes for with and without swirl conditions at varying ϕ , $Re_a = 2000$ and $H = 20$ mm. An equivalence ratio is varied from lean to rich conditions of $\phi = 0.4$ to 1.3 to analyse the results for the fuel lean, stoichiometric and rich conditions. For without swirling IDF, for the lean conditions, the soot free flames are observed for the $\phi = 0.4$ to 0.6. The flame exhibits small amount of soot at $\phi = 0.8$ and 1. Further, an intensity of soot

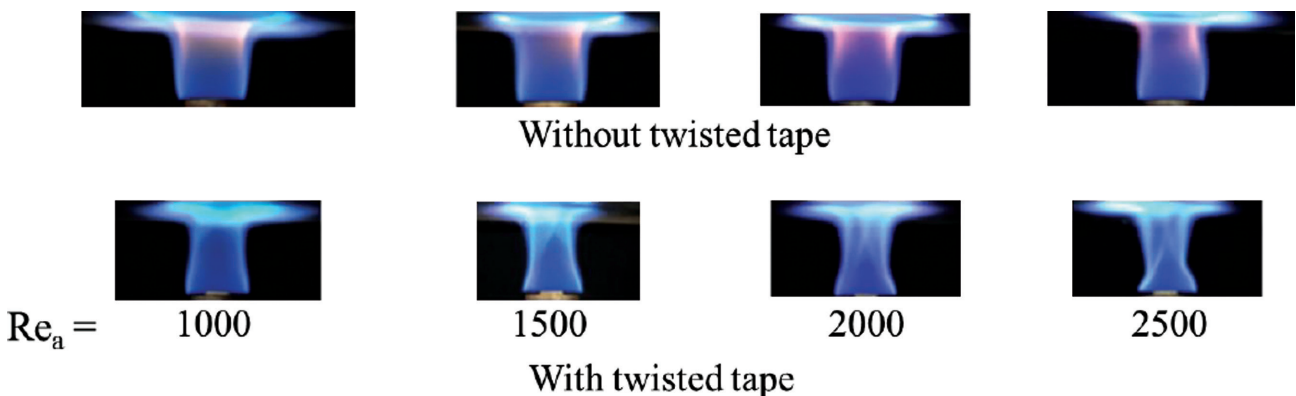


Figure 3. Photos of the non-swirling and swirling coaxial IDF at varying Re_a , $\phi = 1.1$ and $H = 20$ mm.

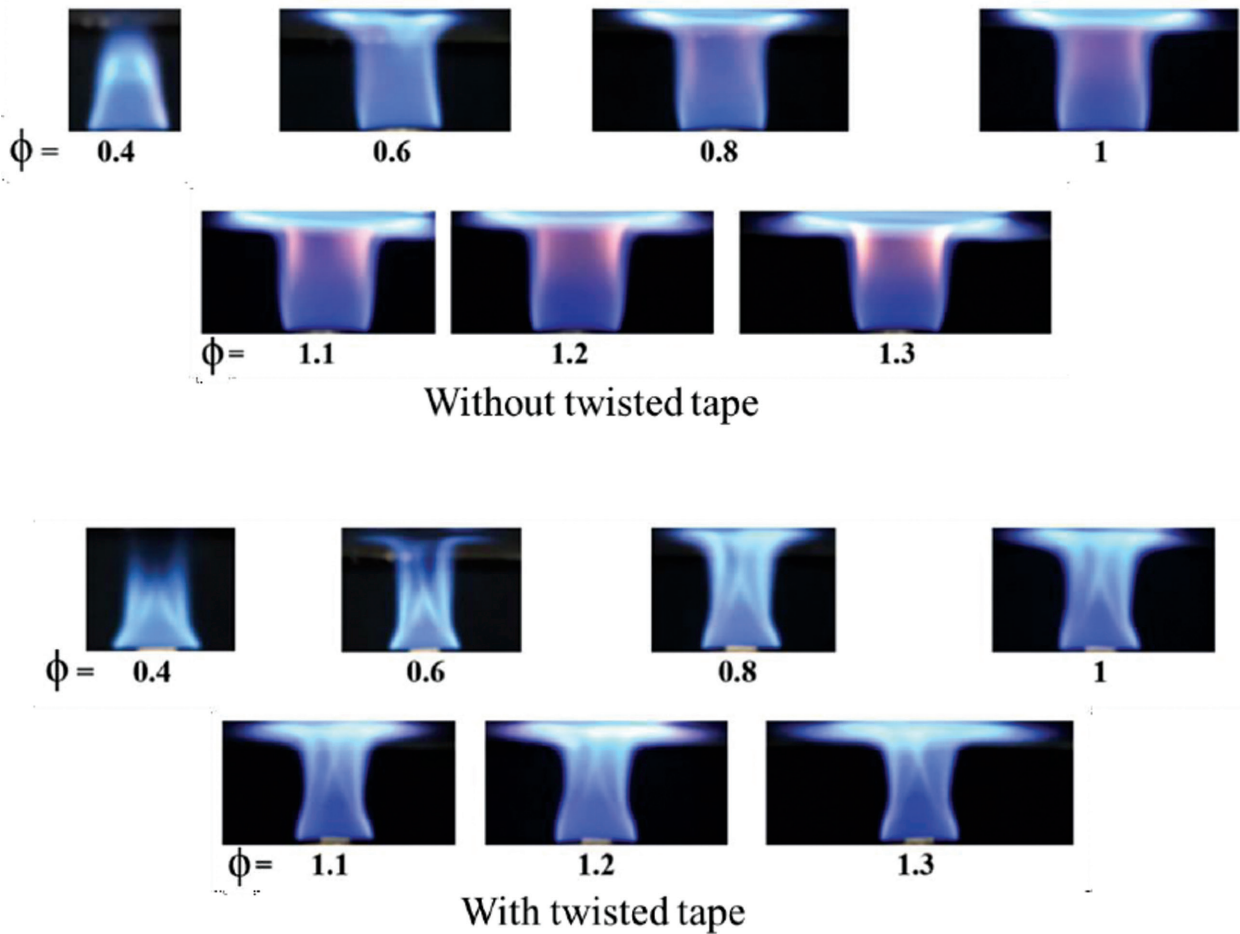


Figure 4. Photos of the non-swirling and swirling coaxial IDF at varying ϕ , $Re_a = 2000$ and $H = 20\text{mm}$.

is higher for the fuel rich conditions of $\phi = 1.1$ to 1.3 . The soot is completely vanished when swirl is provided in the flame jet with the twisted tape of $TR=3$ (corresponding to the swirl number, $S = 0.52$). The swirl reduces the width of the flame and also impingement area on the target surface. An increase in the ϕ , increases the wall jet region, while base flame and neck is un affected for the swirl condition.

An impinging flame shapes of the swirling and non-swirling IDFs operating at varying H , $\phi = 1.1$ and $Re_a = 2000$ are shown in fig. 5. An inverse diffusion flame is the characteristics of a dual structure flame which consists of the base, mixing region and the post combustion zone [26]. The mixing region, where air and fuel interact with each other during the combustion. The soot is observed in this region. The post combustion region consists of an inner reaction cone and also the diffusion layer as shown in the fig. 5. An impingement of the different zones of the IDF flame to the plate depends upon the distance between the burner surface and the target plate. When swirl is provided in an air jet with the help of twisted tape, splitting

of the flame takes place and the flame height is shortened. The swirling flame impingement is obvious only up to the height of $H = 40\text{ mm}$, for the later H , the flame tip touches the target surface.

Heat Flux Distribution

The radial heat flux distributions of a coaxial inverse diffusion flame without and with swirl for varying Re_a , varying ϕ and varying H are investigated. The radial heat flux values are studied within the distance of $R = 75\text{ mm}$ from the point of stagnation. The comparison is given between the swirl and non-swirling conditions.

Effect of an Air Jet Reynolds Number

The local heat flux distribution on an impingement plate for varying Re_a at $\phi = 1.1$ and $H = 20\text{ mm}$ is presented in the fig. 6(a) and (b) for the without and with swirling conditions respectively. In case of non-swirling impingement, the low heat flux value is seen at the stagnation region due to an impingement of an air jet core. The higher heat flux values

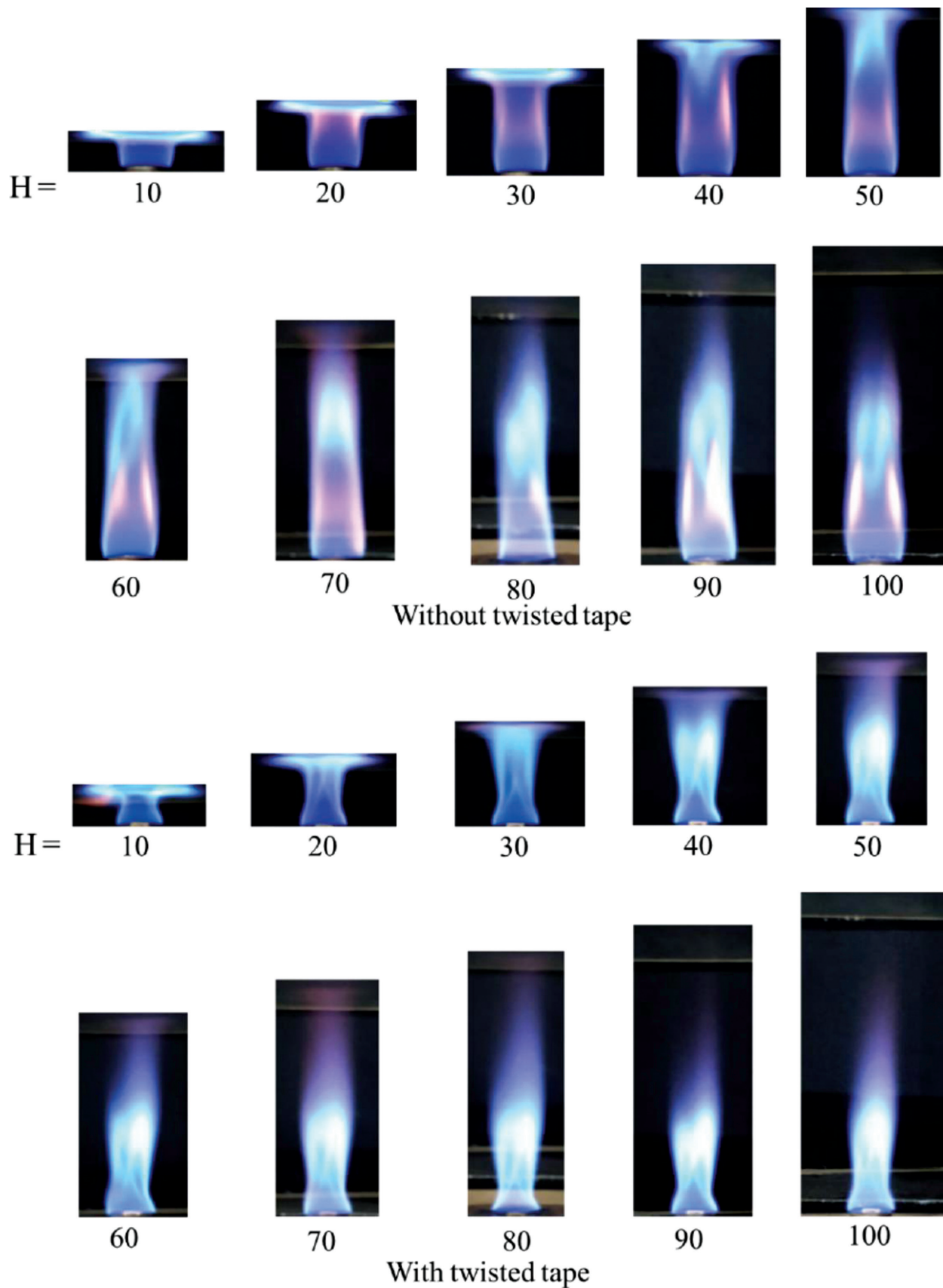


Figure 5. Photos of the non-swirling and swirling coaxial IDF at varying H (mm), $\phi = 1.1$ and $Re_a = 2000$.

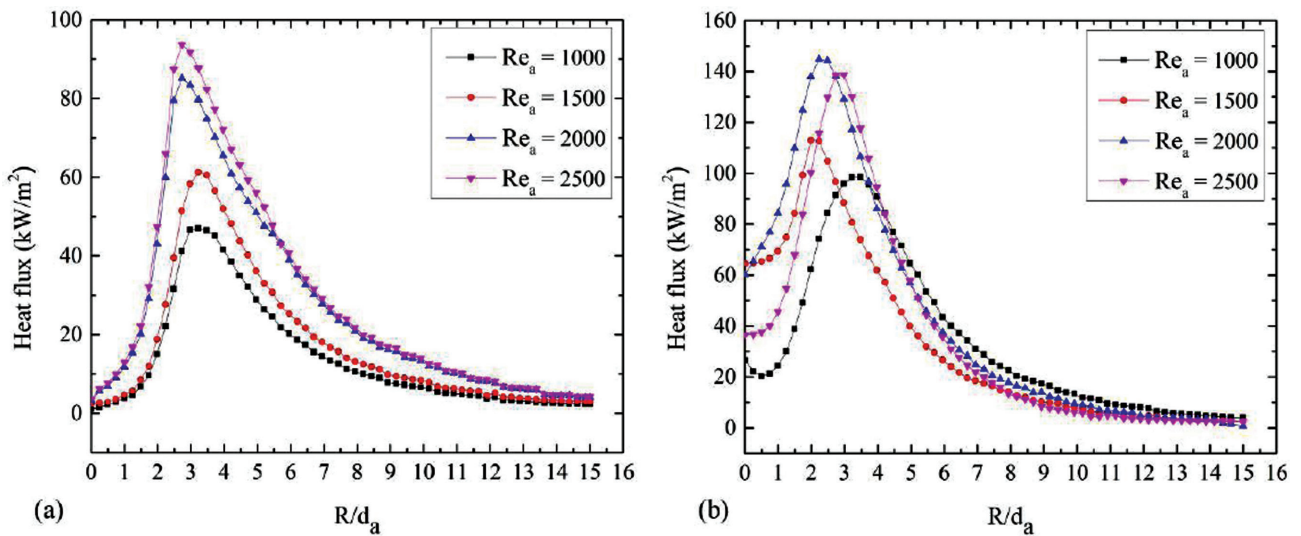


Figure 6. Radial heat flux distributions for varying Re_a for (a) without swirl and (b) with swirl at $\phi = 1.1$ and $H = 20\text{mm}$.

are seen away from the stagnation region between $2 < R/d_a < 4$. This is due the development of combustion in these radial positions. For a constant ϕ and H , as Re_a is increased, both an air and the fuel flow rate increases and hence high heat flux is seen. The peak heat flux values increase from 47 to 94kW/m² when Re_a is increased from 1000 to 2500 for non-swirling conditions. When swirl is provided, there is an increase in the stagnation point and wall jet region heat fluxes as presented in the fig. 6(b). The stagnation point heat fluxes are lower for the $Re_a = 1000$ and 2500 due to an impingement of an air jet core. Figure 7 shows the peak heat flux values for varying Re_a at $\phi = 1.1$ and $H = 20\text{mm}$. The peak heat flux values are higher for swirling impingement at $Re_a = 2000$ and 2500. This is due the greater mixing of an air and fuel, higher level of turbulence and also entrainment of an ambient air, which leads to the combustion of the fuel. There is an enhancement of 48% to 110% in the peak heat flux on the target plate is found for the swirling IDF impingement as compared to non-swirling IDF.

Effect of an Equivalence Ratio

Figure 8(a) and (b) represents an effect of an equivalence ratio (ϕ) on the distributions of radial heat flux values at $Re_a = 2000$ and $H = 20\text{mm}$ for the non-swirl and swirl conditions respectively. Fig. 8(a) shows that an effect of ϕ is negligible on the stagnation point heat flux. Fig. 9 shows the peak heat flux values for varying ϕ at $Re_a = 2000$ and $H = 20\text{mm}$ for the with and without swirl conditions. From the figure it is observed that the peak heat flux increases up to $\phi = 1.2$ and then drops for the non-swirl conditions. The peak heat flux for the non-swirl impingement is observed for $\phi = 1.2$. This is because the richer mixture burns in the radial position, far from the stagnation point and releases

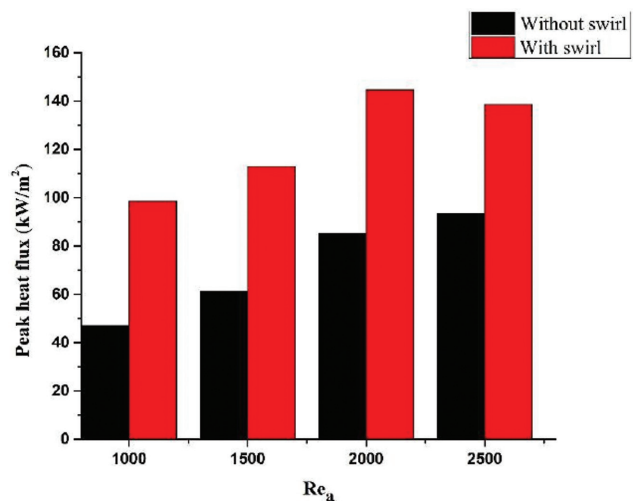


Figure 7. Peak heat flux values for varying Re_a for with and without swirl at $\phi = 1.1$ and $H = 20\text{mm}$.

the maximum heat. There is an increase in the peak heat flux from 29.80kW/m² to 89.37kW/m² when ϕ is increased from 0.4–1.3 as shown in the fig. 9. Fig. 8(b) represents an effect of swirl on the local heat flux distributions along the radius of an impinging plate. Lower heat flux values at the stagnation point are observed for the lean conditions of $\phi = 0.4–0.6$ and for the too rich condition of $\phi = 1.3$. Higher stagnation point heat fluxes are observed for the $\phi = 0.8–1.2$. The swirl results in the stronger entrainment of fuel into an air jet and turbulence enhances the greater mixing and leads to the clean combustion. Fig. 9 shows that the peak heat flux value first increases as ϕ varies from 0.4 to

1.1 and then drops for the $\phi = 1.2$ to 1.3. There is a 13–96% increase in the peak heat flux as compared to without swirl flame impingement. Among the different ϕ , the maximum heat flux is at $\phi = 1.1$. This is due to the peak burning velocity of the methane-air mixture is at slightly fuel rich condition. For the richer condition of $\phi = 1.3$, the air-fuel mixture burns in the radial locations with the help of ambient air and results in high heat flux values in the wall jet region as shown in the fig. 8(b).

Effect of Burner to Target Surface Distance

Figure 10(a) and (b) shows an effect of burner to target surface distance on the radial heat flux distribution at $\phi = 1.1$ and $Re_a = 2000$. For the non-swirling condition, lower stagnation heat fluxes are observed for the $H = 10$ to 40mm. This is due an impingement of the air-fuel mixture before the complete reaction and also the presence of an air jet

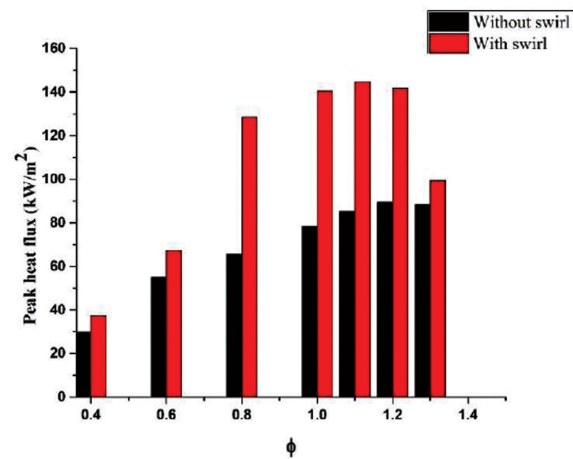


Figure 9. Peak heat flux values for varying ϕ for with and without swirl at $Re_a = 2000$ and $H = 20$ mm.

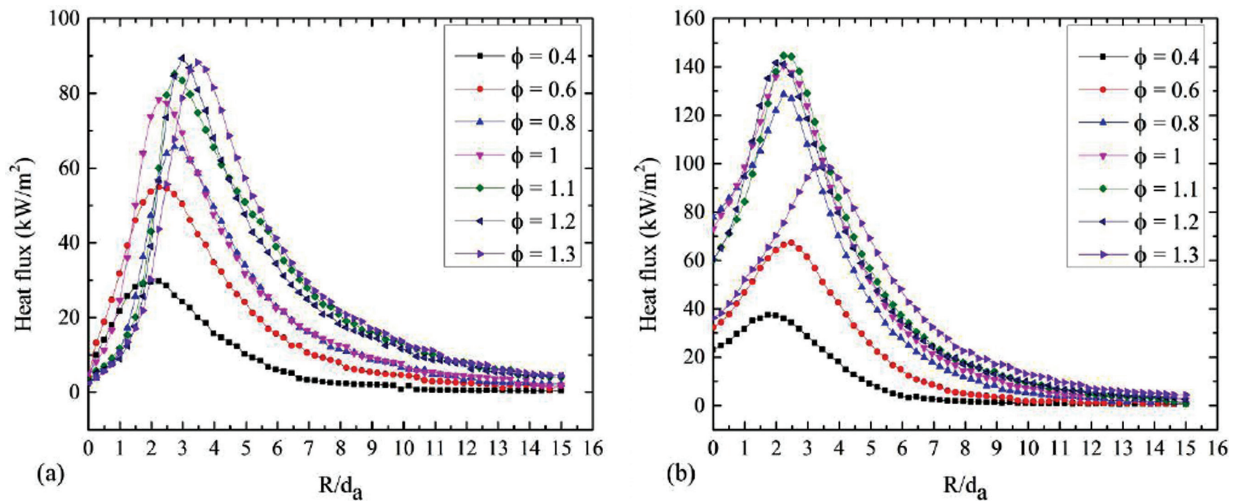


Figure 8. Radial heat flux distributions for varying R/d_a for (a) without swirl and (b) with swirl at $Re_a = 2000$ and $H = 20$ mm.

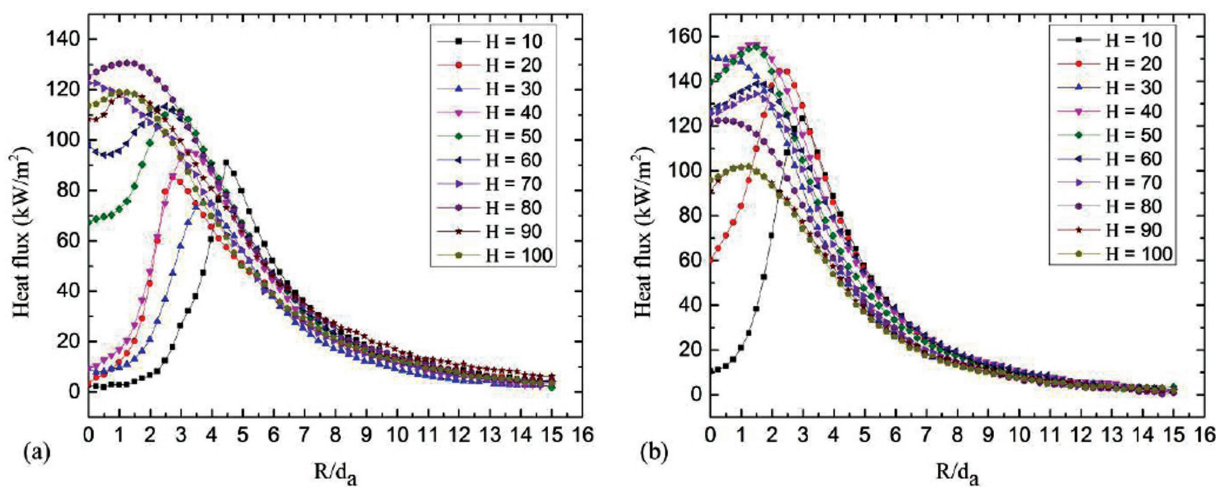


Figure 10. Radial heat flux distributions for varying H (mm) for (a) without swirl and (b) with swirl at $\phi = 1.1$ and $Re_a = 2000$.

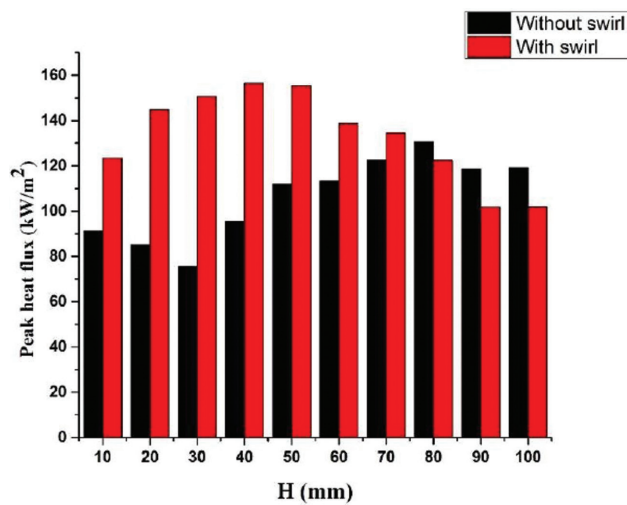


Figure 11. Peak heat flux values for varying H for with and without swirl at $Re_a = 2000$ and $\phi = 1.1$.

core at the center. There is an augmentation of heat flux at the stagnation point for the $H = 50$ to 100 mm, due to an impingement of inner reaction cone of the flame and also the tip of the IDF. In case of swirling flame impingement, the maximum stagnation point heat flux is at $H = 30$ mm. This is due to an impingement of tip of the inner reaction zone where the temperature is highest and this can be seen in the flame shapes of fig. 5. The peak heat flux value shifts near the stagnation region as H is increased from 30 to 100mm. Fig. 11 shows the peak heat flux values for varying H at $\phi = 1.1$ and $Re_a = 2000$. For the swirling impingement, the peak heat flux increases as H is increased from 10–40mm and then drops for the remaining heights. There is an improvement of 9.6–100% in the peak heat flux for between the heights of 10 to 70mm and reduction in the peak heat flux by 6–14% for the remaining heights of 80 to 100mm as compared to non-swirling impingement. The drop in the peak heat flux for the $H = 80$ to 100mm is mainly due to an impingement of post combustion zone of IDF, where the flame temperature is lower and is diluted by the atmospheric air.

CONCLUSION

Experiments are carried out to examine the local heat flux distributions and impinging flame shapes of a coaxial IDF tube burner for the with and without swirl conditions. An effect of air jet Reynolds number (Re_a), an equivalence ratio (ϕ) and the distance between burner to target surface (H) on the local heat flux of swirling IDF is compared with that of non-swirl. The subsequent discussions are made.

- 1) Due to an improper mixing of air and fuel, the non-swirling IDF exhibits the soot formation and longer flame.

- 2) The swirling IDF characterizes with the base flame, neck and the post combustion zone with an inner reaction cone. Swirl created by the twisted tape results in the soot free flames with shorter flame height.
- 3) Swirling effect increases both stagnation region and wall jet region heat flux with an increase in the Re_a . An enhancement of 48–110% in the peak heat flux is found for the swirling flame impingement as compared to non-swirling impingement.
- 4) Swirling IDF showed the higher heat flux on an impingement plate for the stoichiometric and at slightly richer mixture ($\phi = 1, 1.1$) among the ϕ tested. The peak heat flux is at stoichiometric condition ($\phi = 1.1$). The reason is that the peak burning velocity of methane/air mixture is at slightly richer mixture. There is an enhancement of 13–96% in the peak heat flux is seen for the swirling IDF in comparison with non-swirling IDF.
- 5) The heat transfer to an impingement plate depends upon the position of the target plate with respect to inner reaction zone of the IDF. Comparison of swirling and non-swirling IDF reveals that the swirling IDF enhances the peak heat flux by 10–100% for the $H = 10$ to 70mm and then drops by 6–14% for the $H = 80$ to 100mm. An impingement of the inner reaction zone which enhances the heat flux. For the $H = 80$ to 100mm, the swirling flame has not touched the impingement plate and results in lower heat flux.

NOMENCLATURE

Symbol	Meaning
Re_a	Reynolds number of air jet
R	Radial distance from the stagnation point
\dot{m}_a	Mass flow rate of air, kg/s
\dot{m}_f	Mass flow rate of fuel, kg/s
d_a	Diameter of air jet, mm
L	Length of an IDF tube burner, mm
k	Thermal conductivity, W/m k
q''	Heat flux, W/m²
t	Time, sec
T	Temperature, K
Z	Quartz plate thickness, mm
p	Pitch of the twisted tape, mm
w	Twisted tape width, mm

Subscription	Meaning
stoic	Stoichiometric
act	Actual
x	Initial
-	Average value

Greek symbols

α	Thermal diffusivity (m^2/s)
ϕ	Equivalence ratio
μ_a	Absolute viscosity of air (Pa-s)

Abbreviations

A	Air
F	Fuel
TR	Twist ratio
S	Swirl number
IDF	Inverse diffusion flame
IDFs	Inverse diffusion flames
H	Distance between burner surface to target plate (m)

AUTHORSHIP CONTRIBUTIONS

Authors equally contributed to this work.

DATA AVAILABILITY STATEMENT

The authors confirm that the data that supports the findings of this study are available within the article. Raw data that support the finding of this study are available from the corresponding author, upon reasonable request.

CONFLICT OF INTEREST

The author declared no potential conflicts of interest with respect to the research, authorship, and/or publication of this article.

ETHICS

There are no ethical issues with the publication of this manuscript.

REFERENCES

- [1] Sze LK, Cheung CS, Leung CW. Appearance, temperature, and NO_x emission of two inverse diffusion flames with different port design. *Combust Flame* 2006;144:237-248. [\[CrossRef\]](#)
- [2] Mikofski MA, Williams TC, Shaddix CR, Blevins LG. Flame height measurement of laminar inverse diffusion flames. *Combust Flame* 2006;146:63-72. [\[CrossRef\]](#)
- [3] Mahesh S, Mishra DP. Flame stability and emission characteristics of turbulent LPG IDF in a backstep burner. *Fuel* 2008;87:2614-2619. [\[CrossRef\]](#)
- [4] Mahesh S, Mishra DP. Flame structure of LPG-air Inverse Diffusion Flame in a backstep burner. *Fuel* 2010;89:2145-2148. [\[CrossRef\]](#)
- [5] Zhen HS, Choy YS, Leung CW, Cheung CS. Effect of nozzle length on flame and emission behaviors of multi-fuel-jet inverse diffusion flame burner. *Appl Energy* 2011;88:2917-2924. [\[CrossRef\]](#)
- [6] Dong LL, Cheung CS, Leung CW. Combustion optimization of a port array inverse diffusion flame jet. *Energy* 2011;36:2834-2846. [\[CrossRef\]](#)
- [7] Choy YS, Zhen HS, Leung CW, Li HB. Pollutant emission and noise radiation from open and impinging inverse diffusion flames. *Appl Energy* 2012;91:82-89. [\[CrossRef\]](#)
- [8] Miao J, Leung CW, Cheung CS, Huang ZH, Zhen HS. Effect of hydrogen addition on overall pollutant emissions of inverse diffusion flame. *Energy* 2016;104:284-294. [\[CrossRef\]](#)
- [9] Cha MS, Son JW, Yoon SH, Luong HT, Lacoste DA, Sohn CH. Vortex formation mechanism within fuel stream in laminar nonpremixed jet flames. *Combust Flame* 2019;199:46-53. [\[CrossRef\]](#)
- [10] Zhen HS, Leung CW, Cheung CS. Thermal and emission characteristics of a turbulent swirling inverse diffusion flame. *Int J Heat Mass Transf* 2010;53:902-909. [\[CrossRef\]](#)
- [11] Kotb A, Saad H. A comparison of the thermal and emission characteristics of co and counter swirl inverse diffusion flames. *Int J Therm Sci* 2016;109:362-373. [\[CrossRef\]](#)
- [12] Patel V, Shah S. Experimental investigation on flame appearance and emission characteristics of LPG inverse diffusion flame with swirl. *Appl Therm Eng* 2018;137:377-385. [\[CrossRef\]](#)
- [13] Vipul Patel, Rupesh Shah. Effect of swirl and number of swirler vanes on combustion characteristics of methane inverse diffusion flame. *J Mech Sci Technol* 2019;33:1947-1958. [\[CrossRef\]](#)
- [14] Rabee BA. The effect of inverse diffusion flame burner-diameter on flame characteristics and emissions. *Energy* 2018;160:1201-1207. [\[CrossRef\]](#)
- [15] Patel V, Shah R. Analysis of LPG diffusion flame in tube type burner. *J Mech Eng Sci* 2019;13:5278-5293. [\[CrossRef\]](#)
- [16] Tong Y, Liu X, Wang Z, Richter M, Klingmann J. Experimental and numerical study on bluff body and swirl stabilized diffusion flames. *Fuel* 2018;217:352-364. [\[CrossRef\]](#)
- [17] Zhao Z, Yuen DW, Leung CW, Wong TT. Thermal performance of a premixed impinging circular flame jet array with induced-swirl. *Appl Therm Eng* 2009;29:159-166. [\[CrossRef\]](#)
- [18] Hindasageri V, Vedula RP, Prabhu SV. Heat transfer distribution of swirling flame jet impinging on a flat plate using twisted tape. *Int J Heat Mass Transf* 2015;91:1128-1139. [\[CrossRef\]](#)
- [19] Kumar SS, Hindasageri V, Prabhu SV. Local heat transfer distribution on a flat plate impinged by a swirling jet generated by a twisted tape. *Int J Therm Sci* 2017;111:351-368. [\[CrossRef\]](#)

- [20] Kuntikana P, Prabhu SV. Effect of mixture composition on heat transfer characteristics of impinging methane-air flame jets of tube burner equipped with twisted tapes. *Int J Therm Sci* 2017;111:409-422. [\[CrossRef\]](#)
- [21] Singh P, Chander S. Study of flow field and heat transfer characteristics for an interacting pair of counter-rotating dual-swirling impinging flames. *Int J Therm Sci* 2019;144:191-211. [\[CrossRef\]](#)
- [22] Sze LK, Cheung CS, Leung CW. Temperature distribution and heat transfer characteristics of an inverse diffusion flame with circumferentially arranged fuel ports. *Int J Heat Mass Transf* 2004;47:3119-3129. [\[CrossRef\]](#)
- [23] Dong LL, Cheung CS, Leung CW. Heat transfer optimization of an impinging port-array inverse diffusion flame jet. *Energy* 2013;49:182-192. [\[CrossRef\]](#)
- [24] Dong LL, Cheung CS, Leung CW. Characterization of impinging region from an impinging inverse diffusion flame jet. *Int J Heat Mass Transf* 2013;56:360-369. [\[CrossRef\]](#)
- [25] Zhen HS, Leung CW, Cheung CS. A comparison of the thermal, emission and heat transfer characteristics of swirl-stabilized premixed and inverse diffusion flames. *Energy Convers Manag* 2011;52:1263-1271. [\[CrossRef\]](#)
- [26] Zhen HS, Cheung CS, Leung CW, Li HB. Thermal and heat transfer behaviors of an inverse diffusion flame with induced swirl. *Fuel* 2013;103:212-219. [\[CrossRef\]](#)
- [27] Badiger S, Anil TR, Hindasageri V Katti VV. Heat transfer characteristics of an inverse diffusion flame with induced swirl. *J Brazil Soc Mech Sci Eng* 2020;42:252. [\[CrossRef\]](#)
- [28] R.J. Moffat. Using uncertainty analysis in the planning of an experiment. *Journal Fluids Eng* 1985;107:173-178. [\[CrossRef\]](#)